

Electronic Supporting Information (ESI) for:

Edge-on adsorption of multi-chain functional alkanes stabilizes noncovalent monolayers on MoS₂

Tyson C. Davis,[†] Shane R. Russell,[†] Shelley A. Claridge^{*,†,‡}

[†]Department of Chemistry, Purdue University, West Lafayette, IN 47907

[‡]Weldon School of Biomedical Engineering, Purdue University, West Lafayette, IN 47907

**Address correspondence to: claridge@purdue.edu, (phone) 765-494-6070*

Experimental details

Materials. Chloroform (ChromAR grade) was purchased from Macron Fine Chemicals (Center Valley, PA) and used as received. Absolute ethanol (100 % purity) was purchased from Decon Laboratories, Inc. (King of Prussia, PA) and used as received. Manganese(II) chloride tetrahydrate ($\geq 98\%$ dry basis) was purchased from Sigma-Aldrich (St. Louis, MO) and used as received. 1,2-Bis(10,12-tricosadiynoyl)-sn-glycero-3-phosphoethanolamine (diyne PE, $>99.0\%$ purity) was purchased from Avanti Polar Lipids (Alabaster, AL) and 10,12-Pentacosadiynoic acid (PCDA, $\geq 97.0\%$ purity) was purchased from Sigma-Aldrich (St. Louis, MO); both were used as received. Milli-Q water ($\geq 18.2 \text{ M}\Omega\cdot\text{cm}$ resistivity) was used in all experiments. Ultrahigh purity nitrogen was purchased from Indiana Oxygen Company (Indianapolis, IN; 99.999% purity). Self-assembled monolayers of lipids were deposited on either $1 \text{ cm} \times 1 \text{ cm}$ highly oriented pyrolytic graphite (HOPG, MicroMasch, Watsonville, CA) substrates or 1 cm^2 molybdenum disulfide (MoS_2 , SPI Supplies, West Chester, PA) substrates; substrates were freshly cleaved immediately prior to sample deposition. All initial steps in the deposition process were carried out under UV-filtered light to prevent polymerization in solution. PELCO conductive liquid silver paint, standard SEM pin stub mounts, and double coated carbon conductive tape were purchased from Ted Pella, Inc. (Redding, CA).

Langmuir-Schaefer (LS) conversion. LS conversion was performed using a MicroTrough XL Langmuir-Blodgett trough (Kibron Inc., Helsinki, Finland). For the deposition of PCDA, $30 \mu\text{L}$ of a 0.5 mg/ml solution of PCDA in chloroform was deposited on a subphase of deionized water ($\sim 18 \text{ M}\Omega\cdot\text{cm}$). After the small amount of chloroform used for amphiphile transfer was allowed to evaporate (typical equilibration time 15 min), trough barriers were slowly moved inward (4.3 mm/min barrier motion), to increase film uniformity across the trough surface.

At the target average molecular area (*e.g.*, 35 Å²/molecule), the substrate was slowly (5 mm/min) lowered onto the subphase with the cleaved surface facing down, nearly parallel to the liquid interface, using an automated dipper. After 4 min in contact with the liquid interface, the HOPG was gently lifted out of contact with the liquid using the automated dipper at the same speed. The deposition of diyne PE followed the same procedure, utilizing a subphase of 5 mM MnCl₂.

Unless stated otherwise, diacetylene-functionalized amphiphile monolayers prepared using the described procedure were photopolymerized prior to imaging in order to improve monolayer stability. Photopolymerization was performed by 10–360 min of irradiation under a 254-nm 8-W UV lamp with approximately 4 cm between the lamp and the sample surface.

Temperature-controlled LS conversion. To enable temperature controlled LS conversion, a temperature-controlled transfer stage that was reported previously¹ was used. Samples were mounted on the stage utilizing standard 12 mm diameter high quality magnetic stainless steel AFM specimen discs (alloy 430, Ted Pella, Inc.) that mount on a magnet recessed in the body of the stage. To maximize temperature uniformity across the substrate surface, conductive carbon tape was used to affix the back of the substrate to the specimen disc surface. The temperature of the substrate was confirmed using a thermocouple prior to dipping.

Solution processing assays. For washing experiments, lipid films were subjected to a vigorous stream of ethanol delivered via syringe; in a typical washing experiment, 5 mL of solvent was used. Immediately following each solvent wash, the sample was blown dry with ultrahigh purity nitrogen. After solvent rinsing and substrate drying, AFM imaging was performed, imaging the same location before and after washing.

SEM imaging. SEM images were obtained on a FEI NOVA NanoSEM Field Emission SEM or a Teneo VS SEM (FEI Company, Hillsboro Oregon). Microscopy from the FEI NOVA NanoSEM was performed at 5 kV accelerating voltage at a ~ 3 mm working distance, with an aperture of 30 μm , producing a current of ~ 0.896 nA. Images were acquired using a through-the-lens detector (TLD) with an immersion lens. SEM images obtained on the Teneo VS SEM were acquired at a working distance of ~ 5 mm using the segmented in-lens T3 detector. A beam current of 3.2 nA was selected for best resolution image acquisition through a 32 μm diameter aperture with an accelerating voltage of 5 kV. All substrates were affixed to standard SEM pin stub specimen mounts with conductive carbon tape. To further enhance substrate–mount conductivity, a small amount of colloidal silver paint was applied along the perimeter of the substrate from the face down to the underlying pin stub.

AFM imaging. All AFM measurements were performed under ambient conditions using a Bruker (Bruker Instruments, Billerica, MA) MultiMode AFM equipped with an E scanner. The cantilever oscillation phase shift was carefully monitored to ensure the tip was engaged in the attractive mode to improve imaging of lamellar structures within domains. The setpoint ratio was typically maintained between 0.4 and 0.7 and was rarely decreased below 0.4 to avoid tip sweeping effects.

Image analysis. Images were processed using Gwyddion scanning probe microscopy data visualization and analysis software² and ImageJ analysis software³ to perform median line corrections, plane flattening, scar artifact removal, and contrast adjustment.

Energy minimization. Software packages Maestro and Macromodel (Schrödinger, Cambridge MA) were used, respectively, to visualize molecular structures and to perform force field minimizations. Models were minimized using the OPLS_2005 force field, with extended cutoffs

for Van der Waals, electrostatic, and hydrogen bonding interactions. The dielectric constant of the simulation was set to 80.1. Minimizations were performed using the Polak-Ribiere conjugate gradient (PRCG) algorithm and gradient method with 50000 runs and a convergence threshold of 0.05.

Alignment of diynes in stacked phases for polymerization.

In the main manuscript Figure 1, we show a molecular model of diyne PE on MoS₂ in an edge-on adsorption geometry. Here, to facilitate visual inspection, we highlight the positions of the diynes in the two layers of alkyl chains (Fig. S1a); red lines indicate the lower layer of diynes, while gold lines indicate the top layer. Minimized molecular models in Fig. S1b-d illustrate top views of models in which only the bottom layer of diynes has been polymerized (Fig. S1b), only the top layer (Fig. S1c), and both layers (Fig. S1d). The left row of molecules is assembled with the phosphate oriented toward the environmental interface; the right row of molecules has the

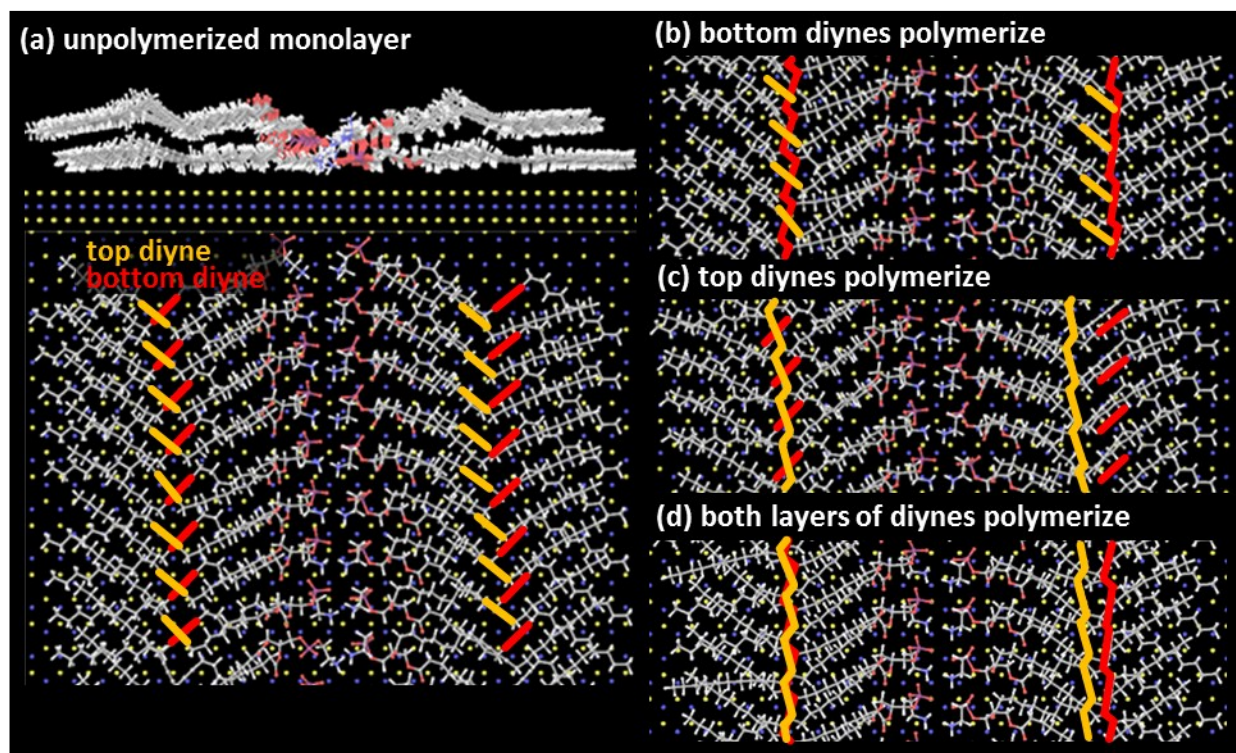


Figure S1. Molecular models of diyne PE in edge-on adsorption geometry, with positions of diynes highlighted in red (bottom layer) and gold (top layer). Each model illustrates a different possible polymerization state of the monolayer: (a) unpolymerized, (b) bottom layer of diynes polymerized, (c) top layer of diynes polymerized, and (d) both layers of diynes polymerized.

phosphate oriented down toward the MoS₂. This difference in assembly leads to a substantial difference in the alignment of the diynes in the two layers across the width of the lamellae, although in both cases the layers of diynes orient at approximately right angles to one another, increasing the likelihood that the two layers polymerize separately. Such behavior would be congruent with the polymerization of diyne phospholipids observed previously in standing phases.⁴

Larger versions of images in main manuscript illustrating differences in domain height and rotation for diyne PE on MoS₂.

In the main manuscript, AFM images illustrate two distinct classes of diyne PE domain heights on MoS₂ that are visible at sub-monolayer coverage. Here, we show a larger version of the image for visual comparison (Fig. S2), highlighting that areas of both phases are visible in the lower-coverage area in the center. The AFM phase images (Fig. S2 inset) shows the lack of lamellar contrast in the lowest topography area, indicating that it represents the MoS₂ substrate. Within the diamondoid vacancy in the monolayer are also regions in which molecules assemble epitaxially on the substrate, with a majority domain height of ~0.4 nm, and local linear protrusions with a total height of 0.6-0.8 nm in comparison with the substrate. It is not possible to completely exclude the possibility that these regions represent a second layer of molecules with face-on orientation. However, the fact that these very small molecular areas are stable toward repeated imaging and do not further consolidate to form a terrace suggests that they are in fact lines of molecules with edge-on adsorption geometries. Fig. S3 shows a larger area of the same substrate with ~80% edge-on adsorption and 4% face-on adsorption, and 16% vacancies.

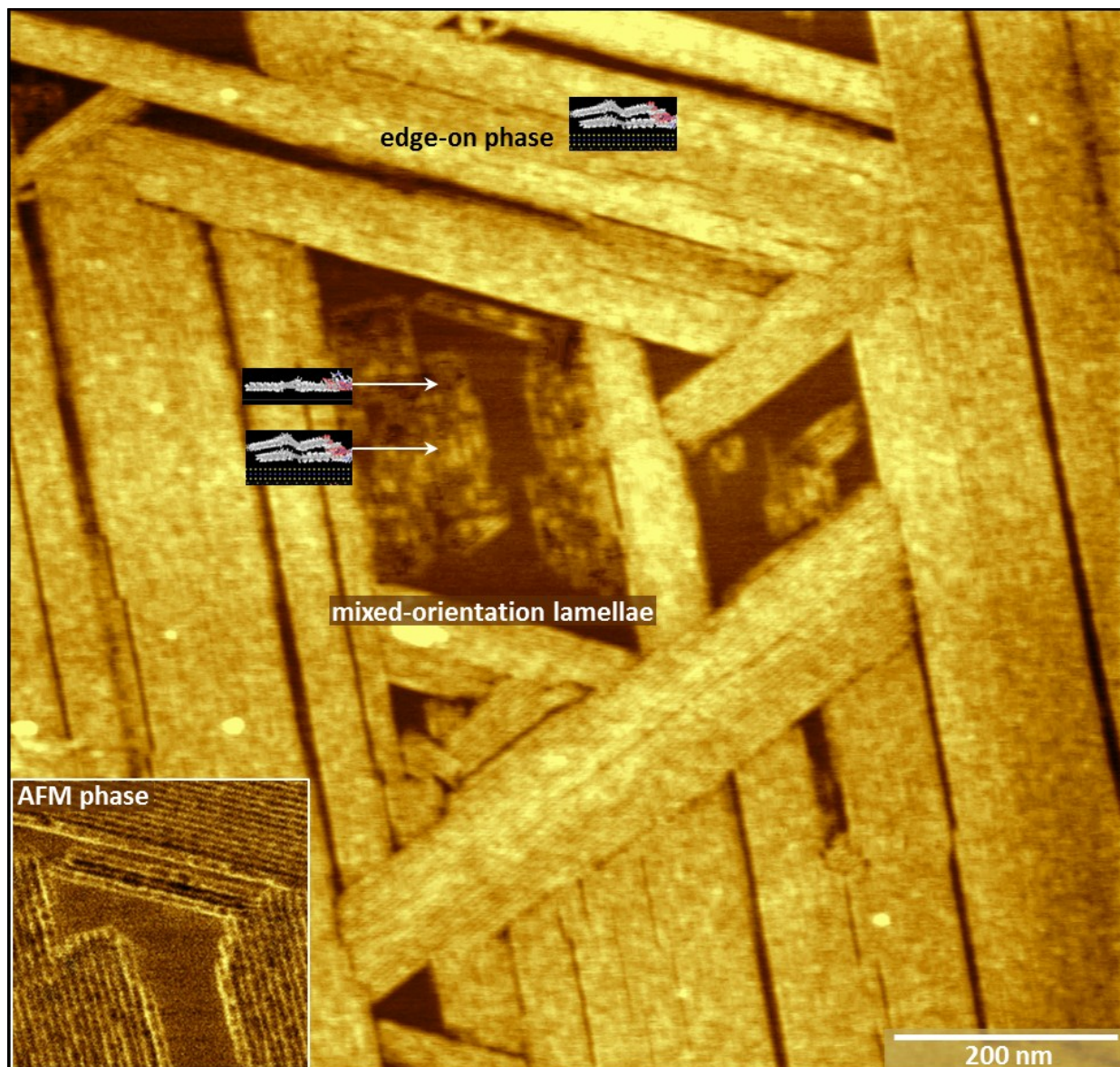


Figure S2. Representative AFM image of diyne PE at sub-monolayer coverage on MoS₂, illustrating domains exhibiting edge-on and face-on adsorption. AFM phase image (inset) shows lack of lamellar contrast in background, indicating that the background represents the MoS₂ substrate.

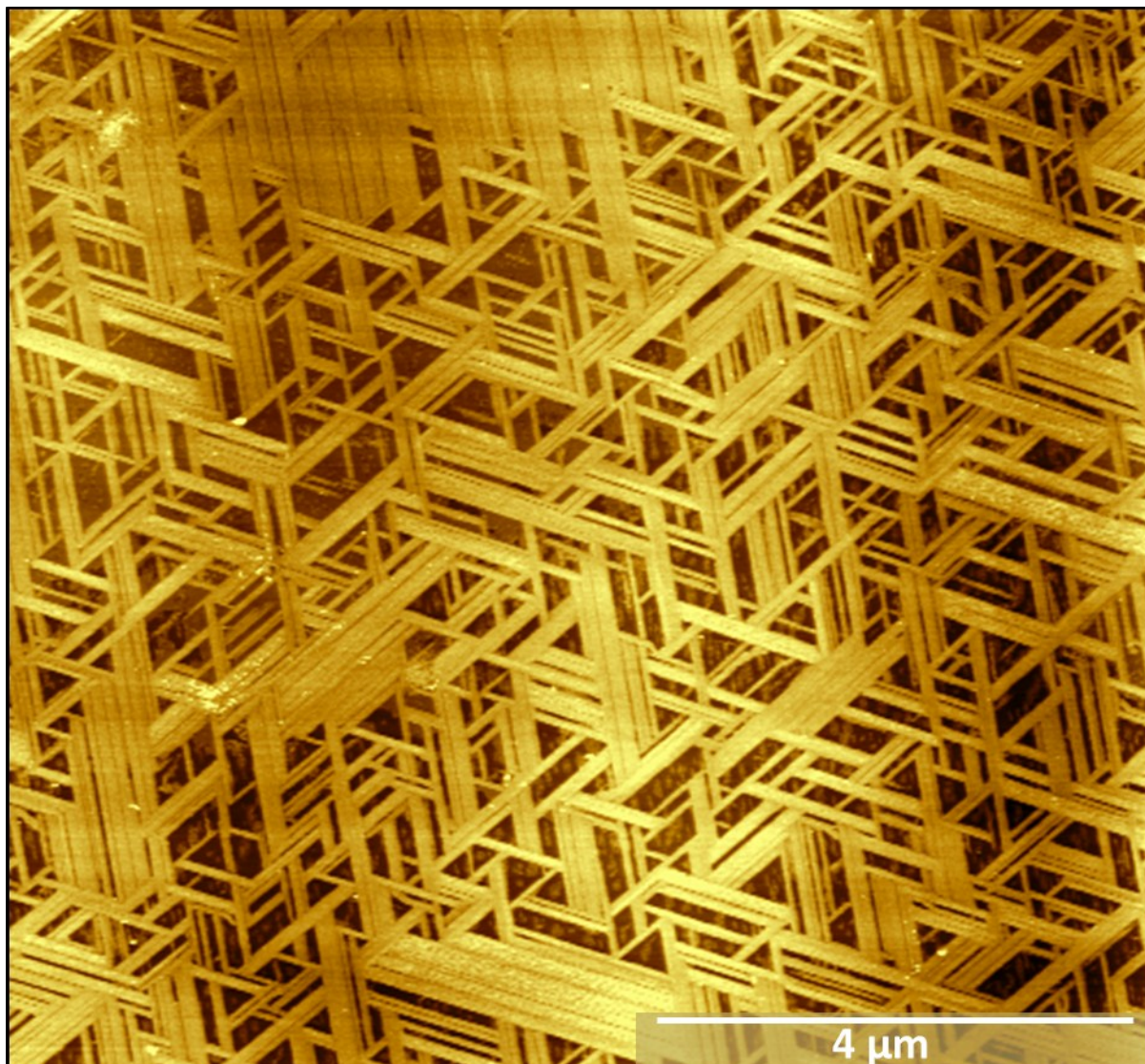


Figure S3. Large-area AFM image of diyne PE on MoS₂ at sub-monolayer coverage. Small domains of molecules in face-on adsorption geometries are visible in the triangular vacancies.

SEM images (Fig. S4) at high coverage also reveal reasonably uniform contrast, consistent with predominantly monolayer coverage. Previously we have found that in areas with significant variations in film thickness, contrast changes are evident in the SEM image, which is evident under some transfer conditions in the thermal screening section presented later in the ESI.

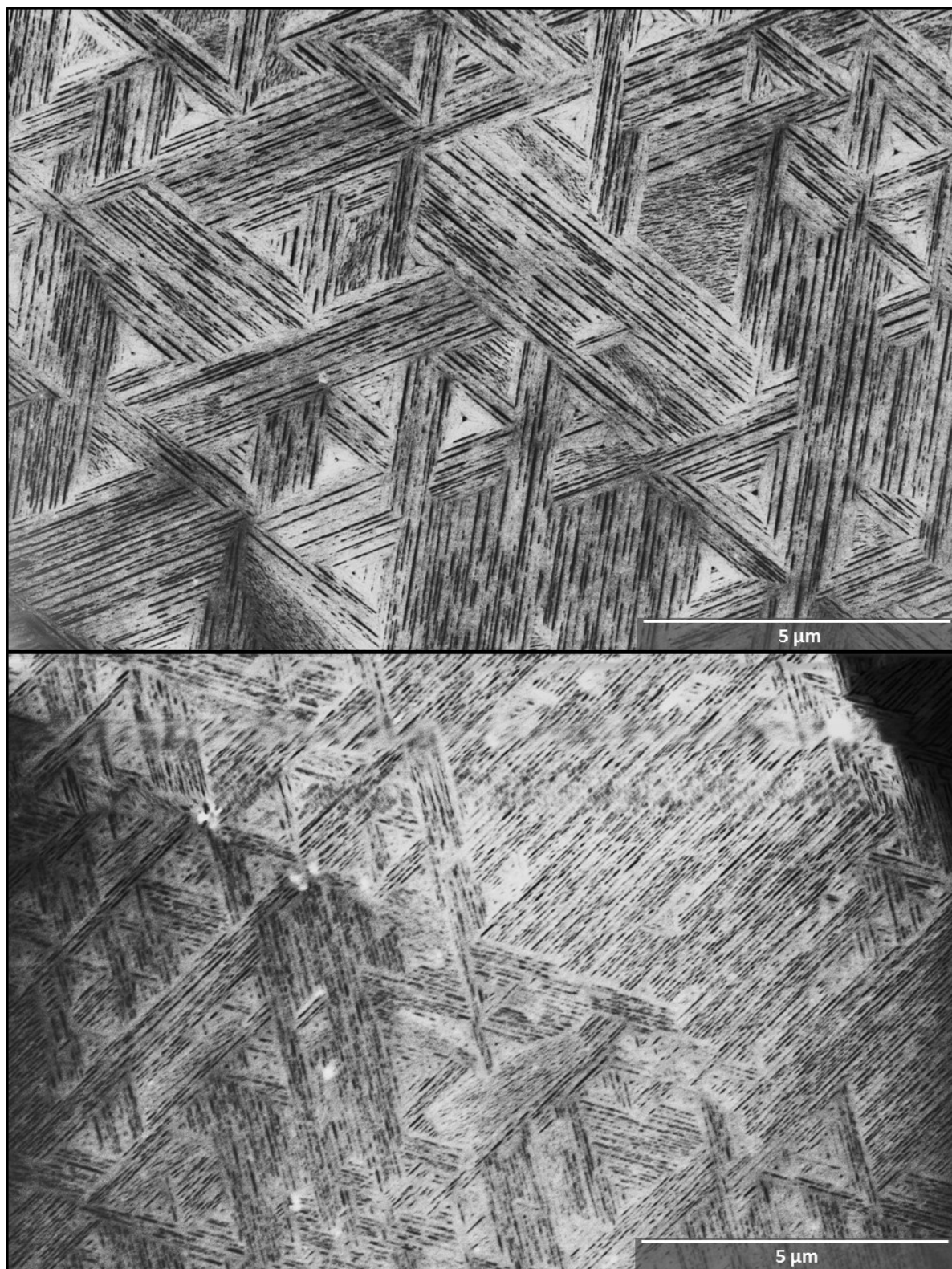


Figure S4. SEM images of diene PE on MoS₂ exhibiting long-range ordering.

Fig. 2e shows a line scan extracted from an image of diyne PE on HOPG; the image from which the line scan is extracted is included below as Fig. S5, with the location of the line scan highlighted in white.

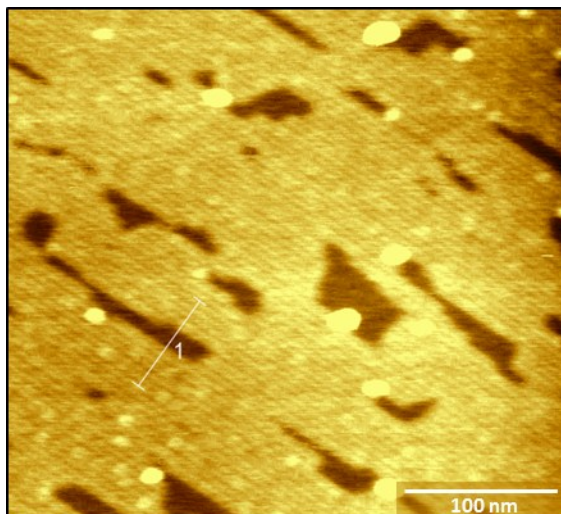


Figure S5. AFM image of diyne PE on HOPG used for line scan in Fig. 2e. Extracted line is highlighted in white.

In the main manuscript, Fig. 5b illustrates that certain domains (color-coded yellow in Fig. 5b) are rotated $\sim 5^\circ$ relative to the main domain alignment direction. Here, we show the original image at larger scale (Fig. S6), to facilitate comparison, with line scans acquired from adjacent rotated domains (inset), to illustrate the small difference in lamellar periodicity (averaged difference ~ 0.3 nm). While drift can also contribute to differences in measured distances, four pairs of domains measured at different angles relative to the fast scan axis reflect similar percentage differences in lamellar periodicity. Domain rotation is also visible in the SEM images in Fig S4.

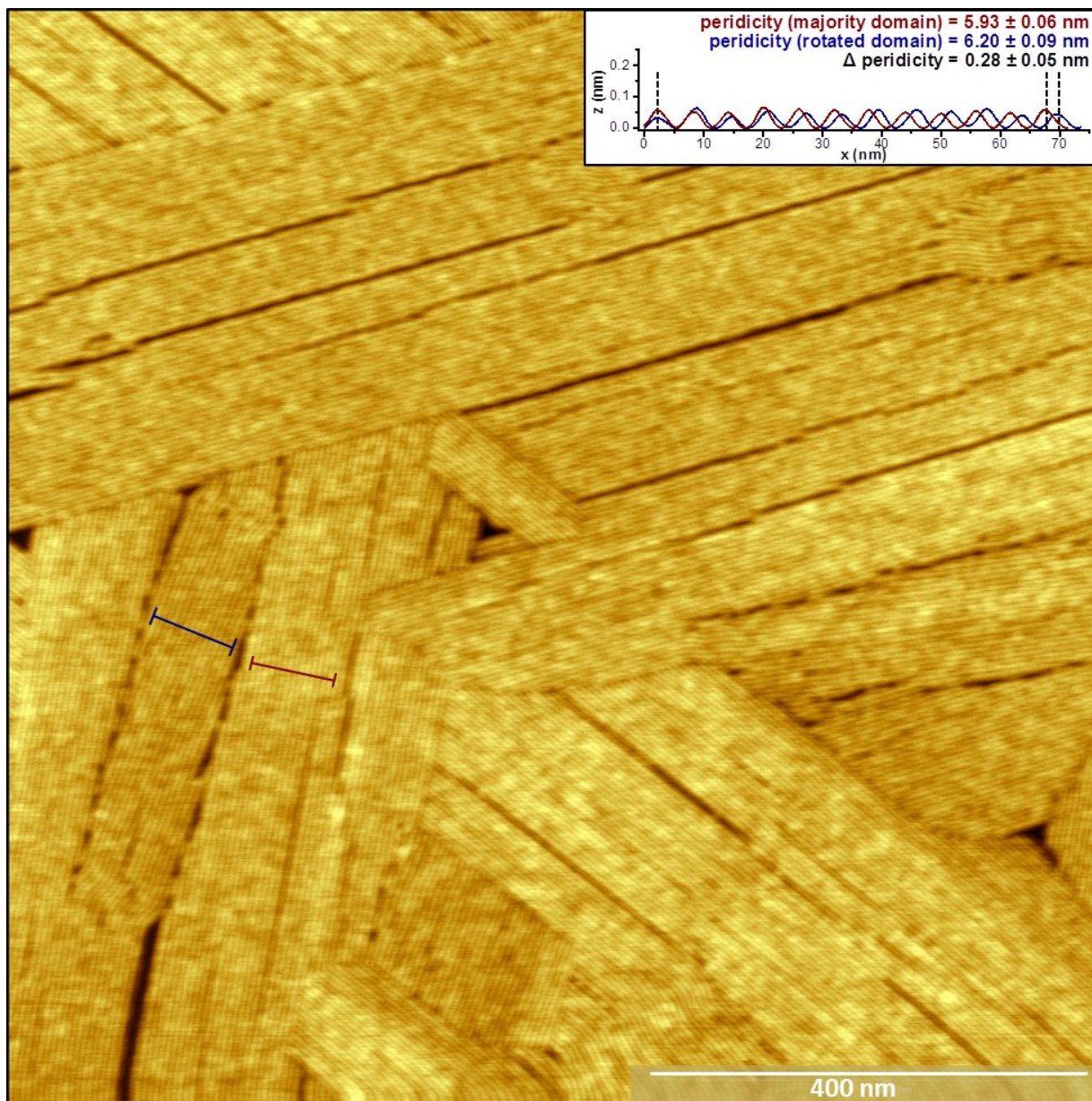


Figure S6. Representative AFM images of diyne PE with a subset of domains rotated relative to the majority domain alignment direction.

Polymerization of diyne PE on HOPG for periods up to 6 h

To examine whether the changes in diyne PE monolayer structure observed in 1 h of polymerization on MoS₂ were substrate-specific, we examined monolayers on HOPG through longer polymerization times. Fig. S7 illustrates diyne PE on HOPG prior to polymerization (Fig.

S7a,b), and after 1 h (Fig. S7c), 2h (Fig. S7d), 3 h (Fig. S7e), and 6 h (Fig. S7f) of UV irradiation. After 1 h, lamellar roughening begins to occur in the monolayer, while after 3 and 6 h, more substantial restructuring is observed, similar to that observed on MoS₂ after 1 h. The images shown were acquired from similar areas of a single sample in sequence.

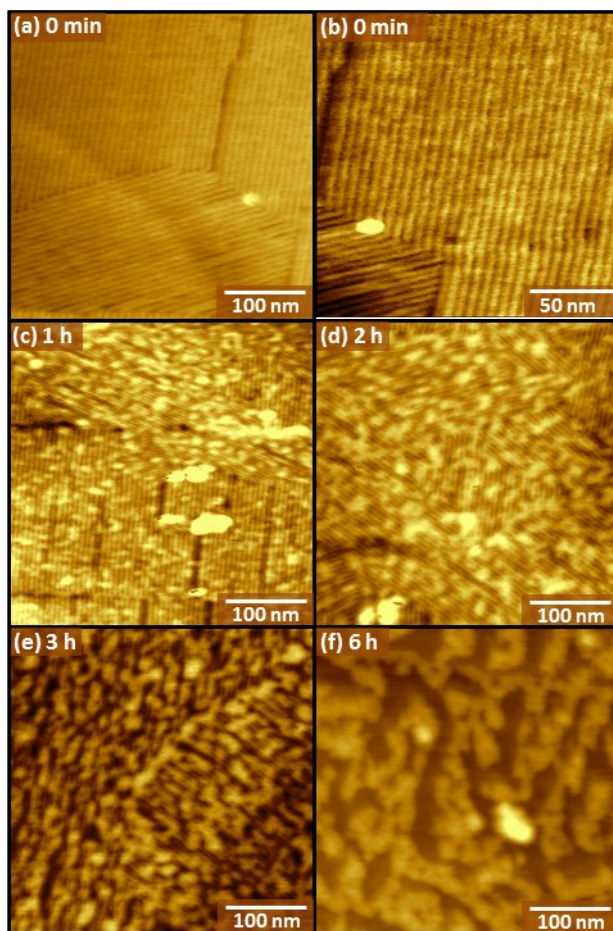


Figure S7. Representative AFM images of diene PE transferred to HOPG, and exposed to UV irradiation for (a,b) 0 min, (c) 1 h, (d) 2 h, (e) 3 h, or (f) 6 h.

Proposed majority and minority domain structures

In the main manuscript, Fig. 5 illustrates a proposed majority domain structure for diene PE on MoS₂, based on differences in linear defects and rotational angles between domains. Here, we

propose a structure and for the minority domain structure, based on minimized molecular models of the three possible lamellar median structures (Fig. S8).

The two possible edge-on adsorption geometries for diyne PE lead to three possible conformations at the lamellar median. Here, we categorize these based on the orientation of the ammonium groups on each side of the median (up | up, up | down, and down | down). Single-point energy calculations for each minimized model indicate the magnitudes of the averaged per-molecule adsorption enthalpies follow the trend up | up > up | down > down | down. This is reasonable given that the N up adsorption geometry brings the entire glycerol backbone into

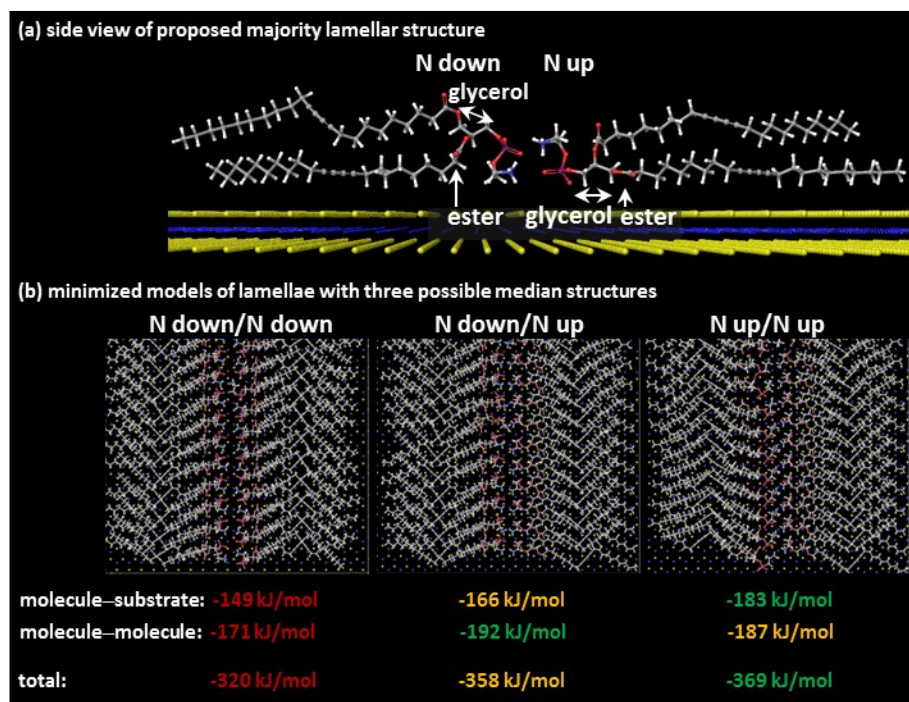


Figure S8. (a) Side view of minimized molecular model of proposed majority lamellar structure, illustrating difference in molecular contact with the substrate in N-down and N-up adsorption geometries. (b) Minimized molecular models of lamellae with three possible median structures (down | down, down | up, and up | up), with calculated molecule-substrate and molecule-molecule interaction strengths.

contact with the substrate, in addition to the phosphate, ester, and acyl chain, resulting in a greater number of van der Waals contact with the substrate.

Conversely, molecule–molecule interactions are slightly stronger for the up | down adsorption geometry, which provides a greater packing density on the substrate. Both N-up and N-down adsorption geometries place terminal methyl groups at different positions relative to the lamellar median, with the result that domains assembled from either up | up or down | down lamellar structures produce inefficient packing of chain ends between lamellae. In contrast, the up | down configuration allows for interdigitation of chain ends.

Structural features observed in SEM are consistent with a domain structure with interlocked edges (*i.e.* N up | N down) for the majority domains. Previously, we have observed that cracking defects form in domains of diynes on HOPG under the electron beam. Small cracks also appear in AFM images of highly ordered domains after polymerization, though the cracks observed in SEM images are greater in width, pointing to the likelihood of some additional restructuring under the electron beam. In SEM images of diyne PE on MoS₂, the majority domain structure exhibits long narrow defects even prior to polymerization, but does not develop additional defects under the electron beam. In contrast, the minority domains develop small linear cracks similar to the polymerization-induced cracking observed previously on HOPG.

Both AFM and SEM images reveal a 5-10° rotational offset between the lamellar axes of the majority and minority domains. Again, this would be consistent with a shift from down | up to up | up lamellar median, as shown in Fig. S9.

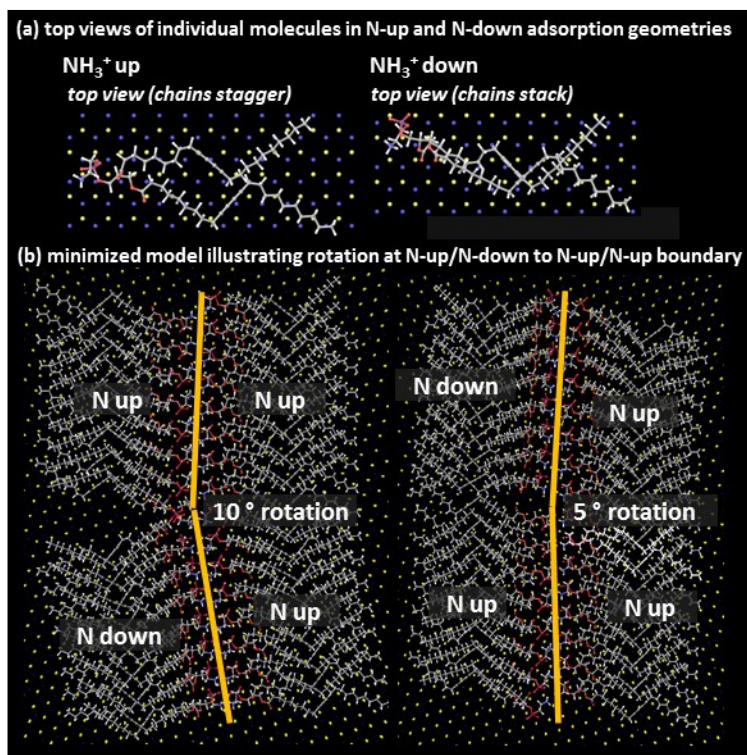


Figure S9. (a) Top views of N-up and N-down adsorption geometries, illustrating difference in chain stacking. (b) Minimized molecular models illustrating rotation at boundary between N-up/N-down and N-up/N-up assembly.

Representative SEM images for transfer of diyne PE to MoS₂ at substrate temperatures 30–90 °C

Transfer of dual chain amphiphiles to MoS₂ across a range of temperatures is compared in Figs. S10–S11. In these experiments, the subphase was held at 30 °C, and the substrate was held at the stated temperature using a custom-built thermally controlled dipper reported previously.¹ Each row in Figs. S10–S11 comprises three representative SEM images (scale bars

100 μm , left, to 1 μm , right) acquired from substrates held at the temperature indicated in the left panel. Images on the left illustrate large-scale features that typically arise from Langmuir film structure; images on the right illustrate lamellar and other domain structures produced at the specified transfer condition. To compare the effect of Langmuir film packing on transfer to MoS_2 , transfer was tested at two Langmuir film packing densities: 20 $\text{\AA}^2/\text{chain}$ (Fig. S10) and 35 $\text{\AA}^2/\text{chain}$ (Fig. S11). These points were chosen to also enable comparison with transfers to HOPG performed previously.^{1,5-7}

At elevated temperatures and packing densities of 20 $\text{\AA}^2/\text{chain}$, lamellar domains are observed for transfers to MoS_2 , with large (>1 μm edge length) domains at 50–70 $^\circ\text{C}$ (Fig. S10b,c). In contrast, lamellar domain assembly on MoS_2 is minimal for transfer from Langmuir films at 35 $\text{\AA}^2/\text{chain}$ or greater (Fig. S11). Higher defect densities in Langmuir films at these $\text{\AA}^2/\text{chain}$ values likely increase transfer rates, and may also permit increased transfer of water from the subphase; both factors could impede assembly of stable lamellar domains on MoS_2 , which is more hydrophilic than HOPG.

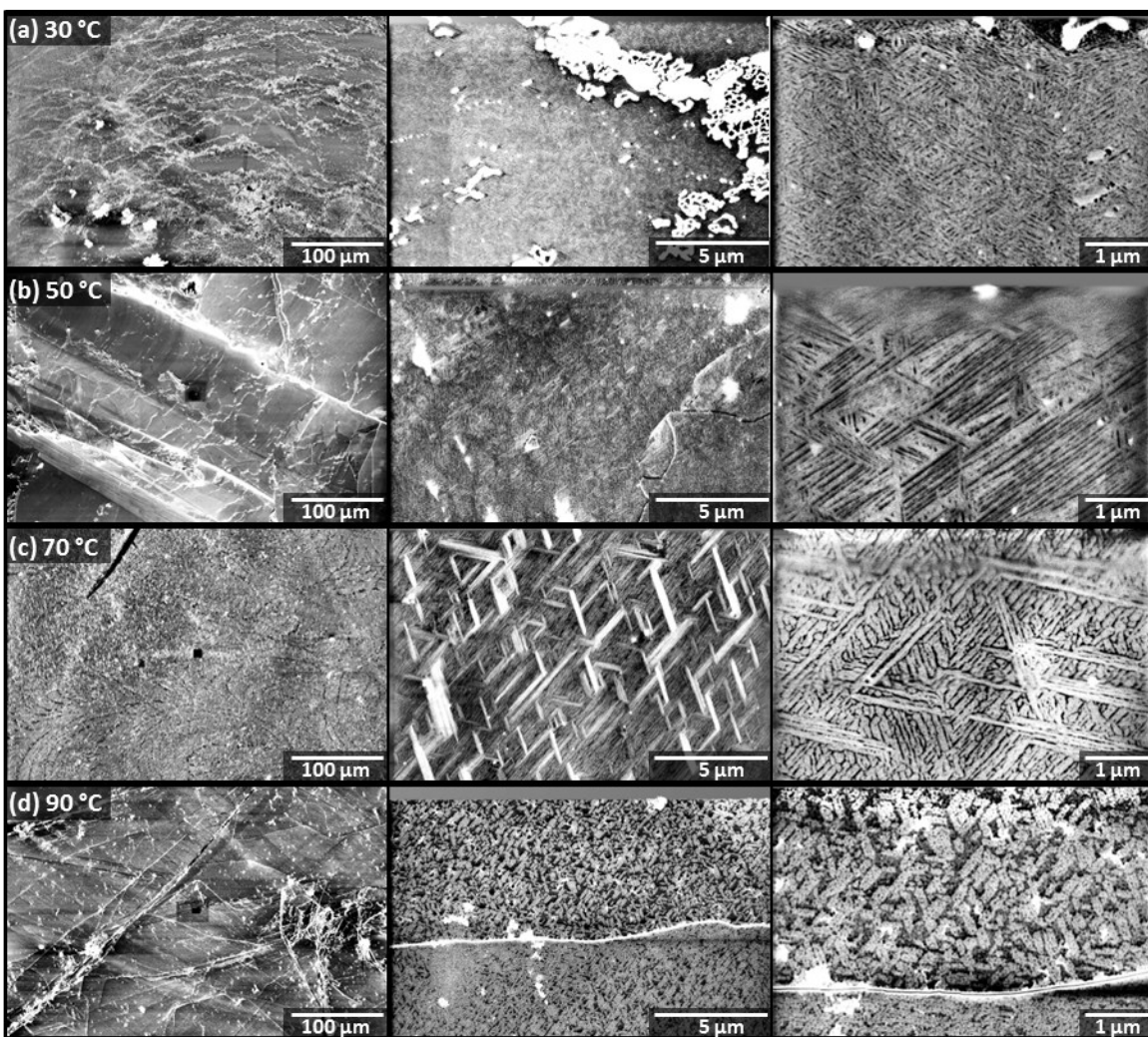


Figure S10. Representative SEM images of diene PE transferred to MoS₂ from Langmuir films with a packing density of 20 Å²/chain and a subphase temperature of 30 °C. Substrate was held at a dipper setpoint temperature of (a) 30 °C, (b) 50 °C, (c) 70 °C, or (d) 90 °C. Each row comprises images at three different scales for the substrate temperature stated in the left panel.

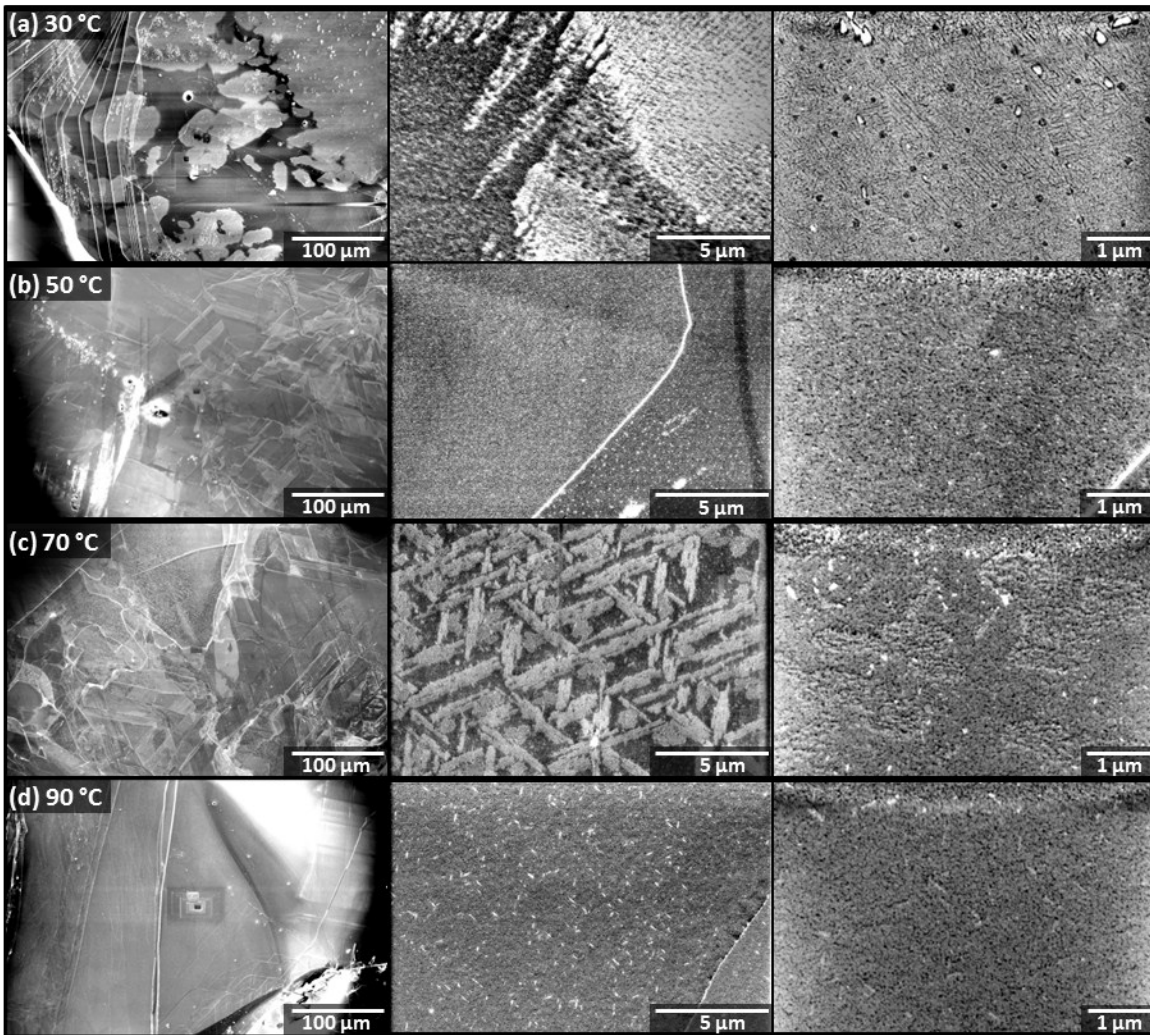


Figure S11. Representative SEM images of diene PE transferred to MoS₂ from Langmuir films with a packing density of 35 Å²/chain and a subphase temperature of 30 °C. Substrate was held at a dipper setpoint temperature of (a) 30 °C, (b) 50 °C, (c) 70 °C, or (d) 90 °C. Each row comprises images at three different scales for the substrate temperature stated in the left panel.

Representative SEM images for transfer of PCDA to MoS₂ and HOPG at substrate temperatures 30–90 °C

Transfer of single chain amphiphiles to MoS₂ across a range of temperatures is compared in Figs. S12-S13. In these experiments, the subphase was held at 30 °C, and the substrate was held at the stated temperature using a custom-built thermally controlled dipper reported previously.¹ Each row in Figs. S12-S13 comprises three representative SEM images (scale bars 100 μm, left, to 1 μm, right) acquired from substrates held at the dipper setpoint temperature stated in the left panel. Images on the left illustrate large-scale features that typically arise from Langmuir film structure; images on the right illustrate lamellar and other domain structures that result from the specified transfer condition. To compare the effect of Langmuir film packing on transfer to MoS₂, transfer was tested at two Langmuir film packing densities: 20 Å²/chain (Fig. S12) and 35 Å²/chain (Fig. S13). Transfer of PCDA to MoS₂ under a similar range of conditions to those utilized for diyne PE (Fig. S10-S11) produced high surface coverage, but not large lamellar domains similar to those observed for diyne PE.

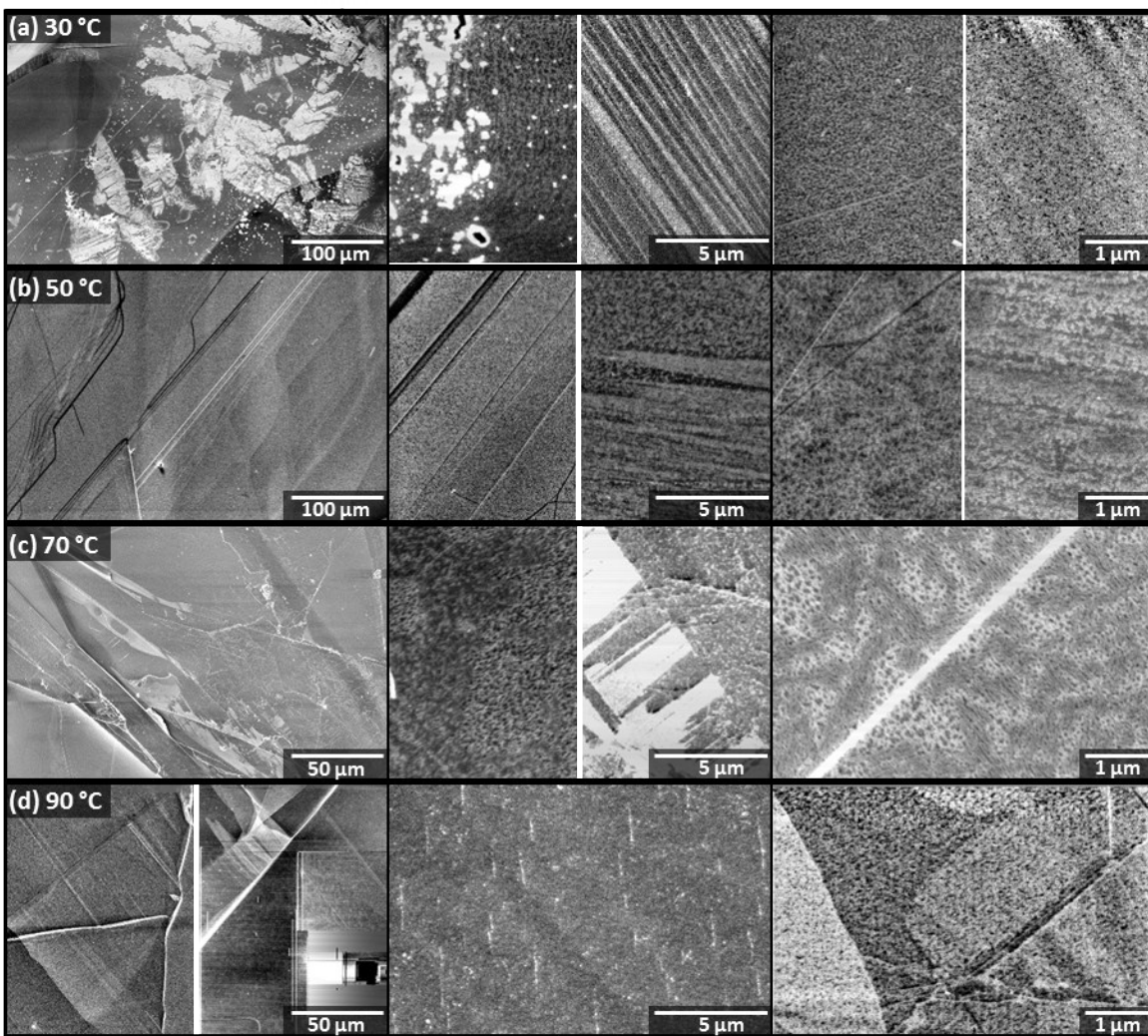


Figure S12. Representative SEM images of PCDA transferred to MoS₂ from Langmuir films with a packing density of 20 Å²/chain and a subphase temperature of 30 °C. Substrate was held at a dipper setpoint temperature of (a) 30 °C, (b) 50 °C, (c) 70 °C, or (d) 90 °C. Each row comprises images at three different scales for the substrate temperature stated in the left panel.

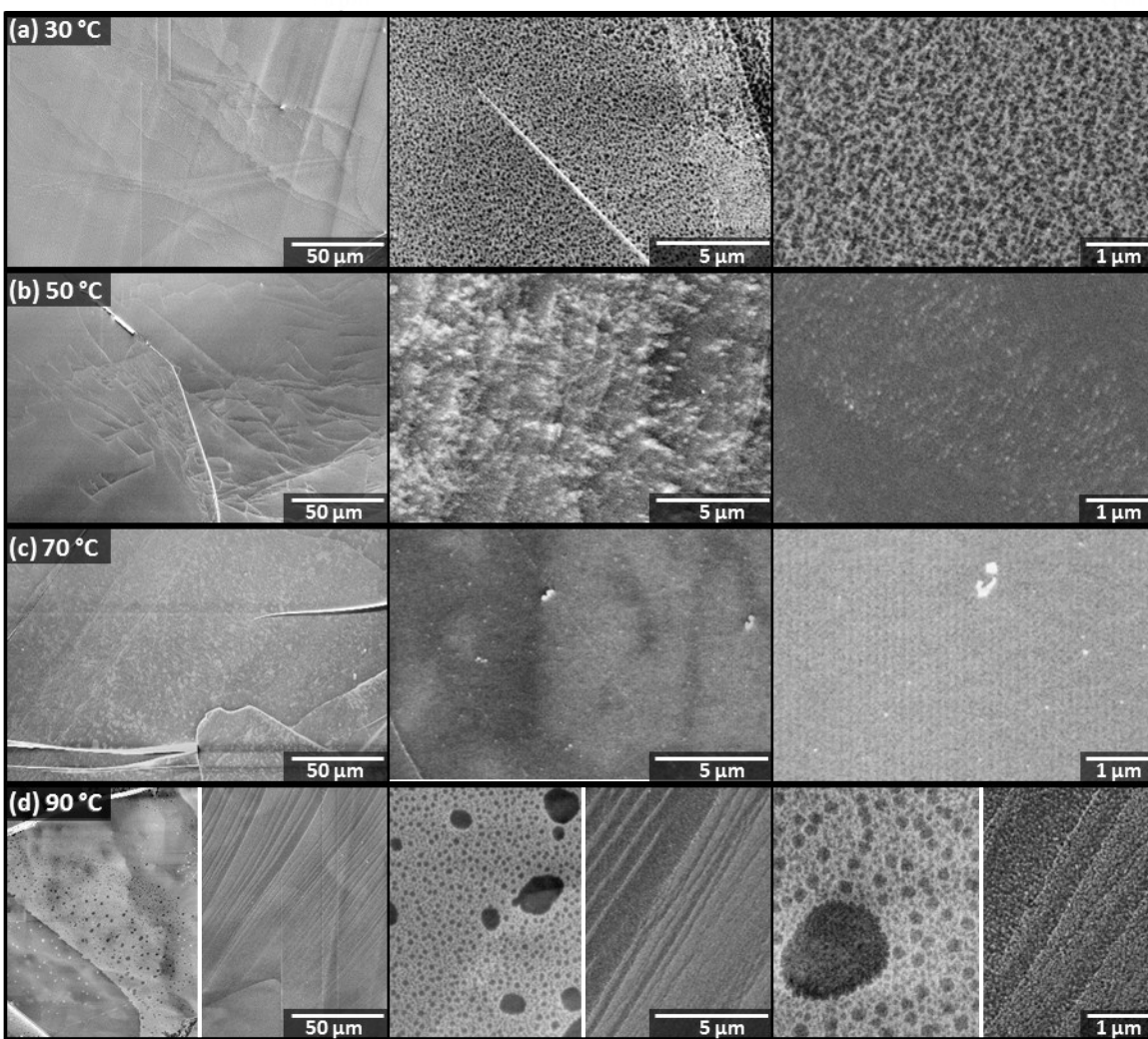


Figure S13. Representative SEM images of PCDA transferred to MoS₂ from Langmuir films with a packing density of 35 Å²/chain and a subphase temperature of 30 °C. Substrate was held at a dipper setpoint temperature of (a) 30 °C, (b) 50 °C, (c) 70 °C, or (d) 90 °C. Each row comprises images at three different scales for the substrate temperature stated in the left panel.

Representative SEM images for solution deposition of PCDA and diyne PE on HOPG and MoS₂. Deposition of amphiphiles from solutions in organic solvent is an experimentally expedient method for noncovalent functionalization. Here, we compare SEM images acquired from HOPG and MoS₂ substrates functionalized with either PCDA or diyne PE deposited from solution. Molecules were deposited on both substrates from dilute solutions (0.0025 mg/mL in

3:2 (v:v) hexane:isopropanol), onto substrates heated to 90 °C, conditions which we have used previously to achieve μm -scale domains of both amphiphiles on HOPG. Fig. S14 shows representative images of MoS_2 functionalized with PCDA, with scale bars ranging from 100 μm to 2 μm . At micrometer scales, significant aggregates are observed on the surface. When diyne PE is deposited on MoS_2 , large areas of both ordered lamellar phases (Fig. S15) and standing phases (Fig. S16) are typically observed, with relatively low surface coverage in the areas of lamellar assembly (linear features in Fig. S15b–d). Fig. S17 shows representative images of HOPG and MoS_2 functionalized with PCDA (Fig. S17a,b) or diyne PE (Fig. S17c,d). When deposited from 0.15 mg/mL in 3:2 (v/v) hexane/isopropanol, surface coverage is overall higher, but significant areas of standing phase are present.

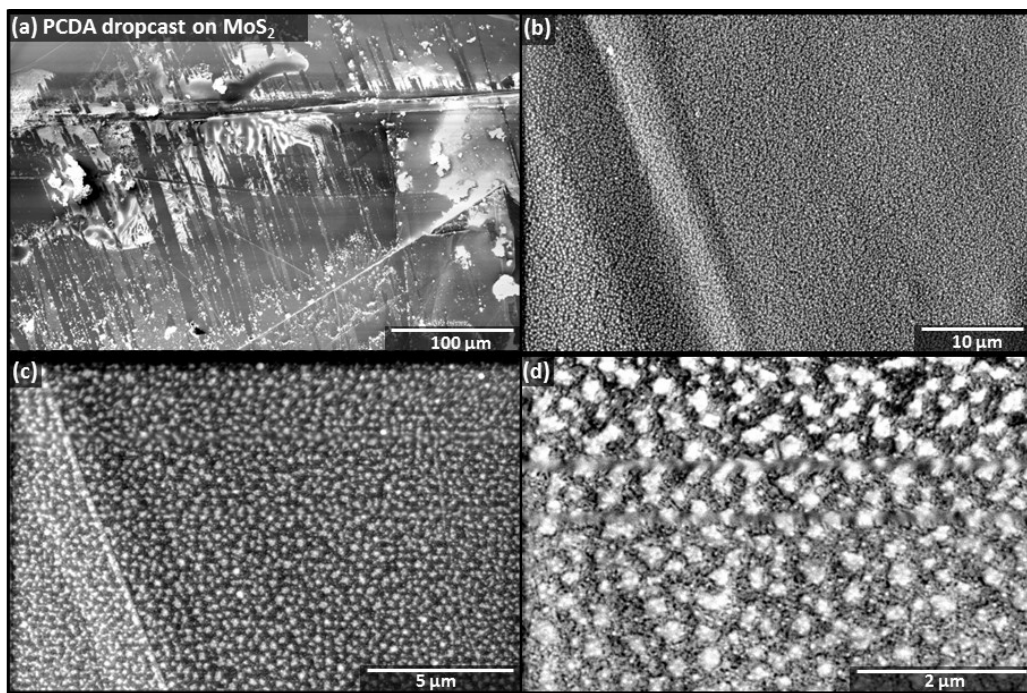


Figure S14. SEM images of PCDA deposited on MoS_2 from 0.0025 mg/mL PCDA in 3:2 (v/v) hexane/isopropanol.

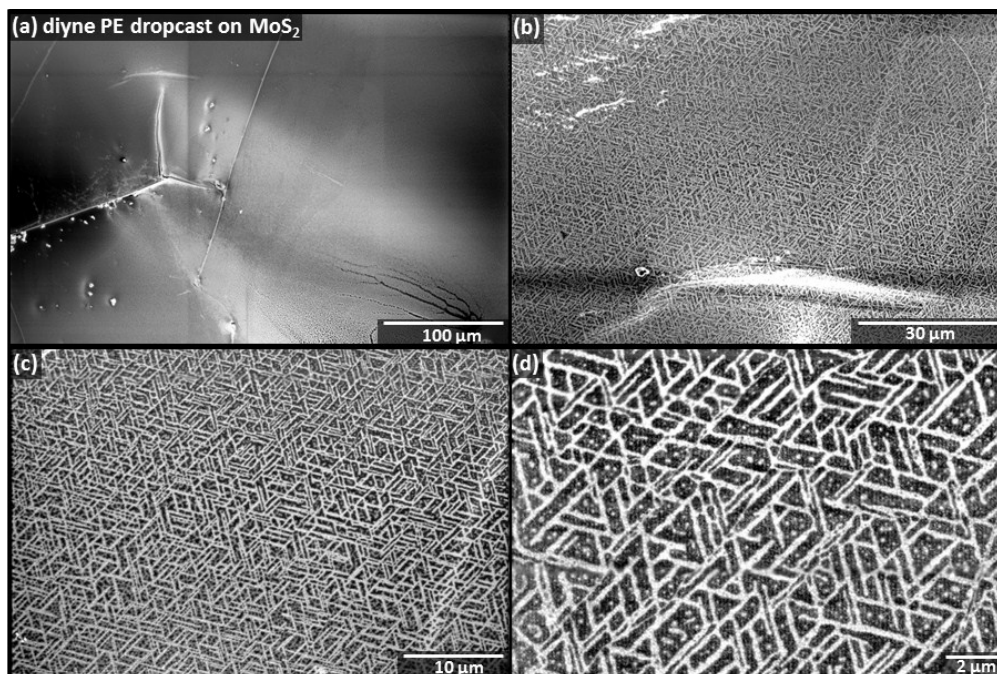


Figure S15. SEM images of diyne PE deposited on MoS₂ from 0.0025 mg/mL diyne PE in 3:2 (v/v) hexane/isopropanol.

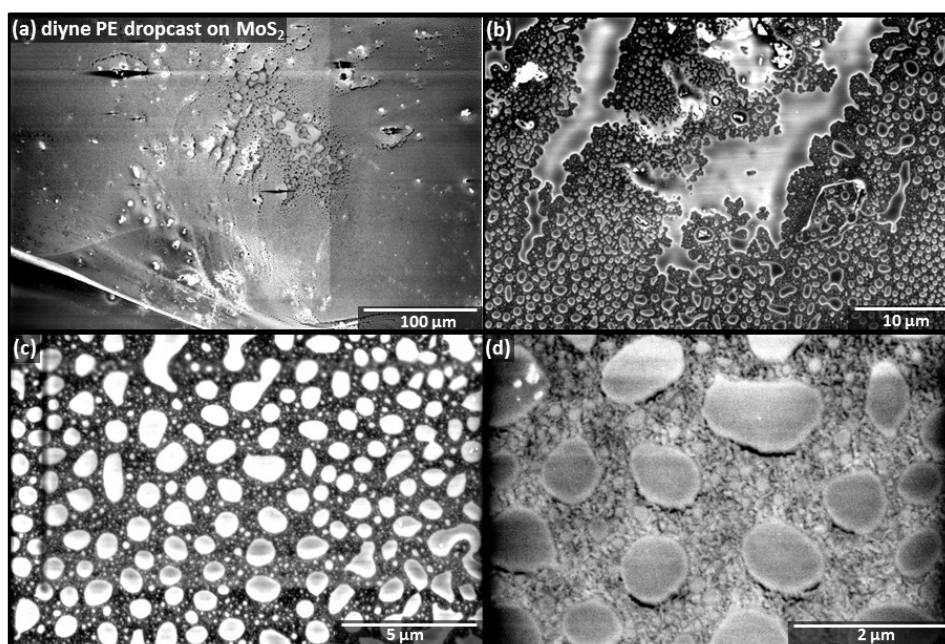


Figure S16. Representative SEM images of diyne PE deposited on MoS₂ from 0.0025 g/mL diyne PE in 3:2 (v/v) hexane/isopropanol. Substrates typically exhibit areas of both lying down phases (similar to Fig. S12), and standing phases (shown here).

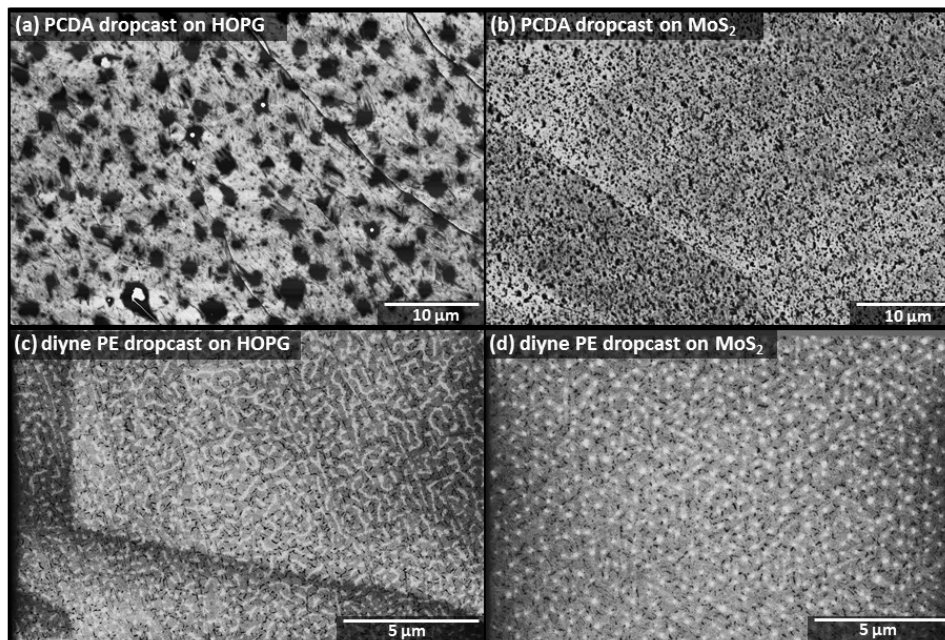


Figure S17. Representative SEM images of (a,b) PCDA and (c,d) diyne PE deposited on MoS₂ from 0.15 mg/mL solution in 3:2 (v/v) hexane:isopropanol. Areas that appear dark in (a) and (b) are large aggregates of PCDA that do not produce strong scattering.

Additionally, we compared results obtained for slowly removing substrates from a dilute solution of each molecule (dip-coating). Figure S18 compares results of the three film preparation procedures for the two molecules and substrate types tested. While dip-coating produces the most even surface coverage, thermally controlled LS transfer produces large, highly ordered molecular domains while maintaining reasonable uniformity of surface coverage.

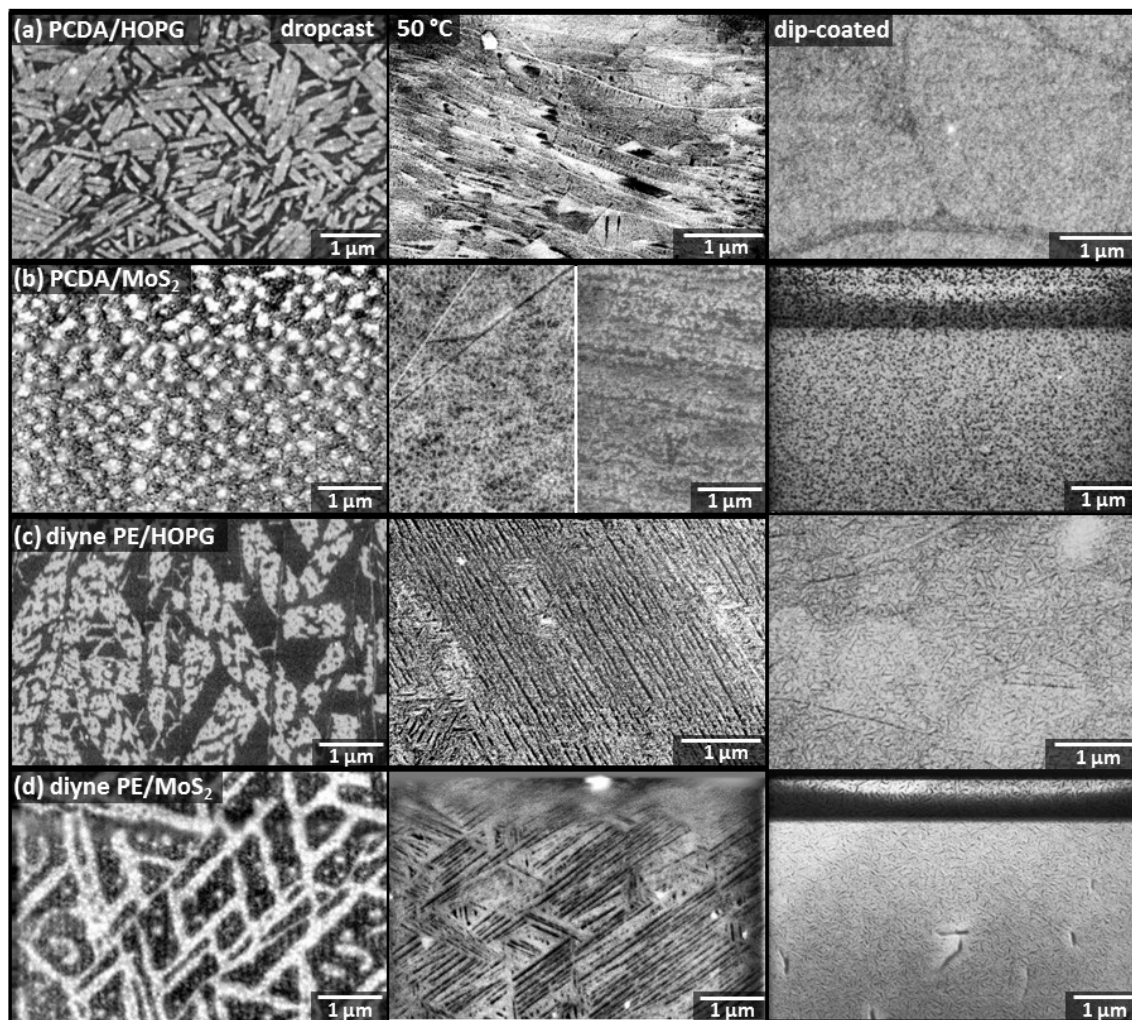


Figure S18. Representative SEM images of (a) PCDA assembled on HOPG, (b) PCDA assembled on MoS_2 , (c) diyne PE assembled on HOPG, and (d) diyne PE assembled on MoS_2 , via the stated surface preparation method: (left) dropcasting, (center) thermally controlled LS transfer with a dipper set point temperature of $50\text{ }^\circ\text{C}$, or (right) dip-coating.

References cited

1. Hayes, T. R.; Bang, J. J.; Davis, T. C.; Peterson, C. F.; McMillan, D. G.; Claridge, S. A., Multimicrometer Noncovalent Monolayer Domains on Layered Materials through Thermally Controlled Langmuir-Schaefer Conversion for Noncovalent 2D Functionalization. *ACS Appl. Mater. Interf.* **2017**, *9*, 36409–36416.
2. Nečas, D.; Klapetek, P., Gwyddion: An Open-Source Software for SPM Data Analysis. *Cent. Eur. J. Phys.* **2012**, *10*, 181-188.
3. Schneider, C. A.; Rasband, W. S.; Elicieri, K. W., NIH Image to Imagej: 25 Years of Image Analysis. *Nat. Methods* **2012**, *9*, 671-675.
4. Lopez, E.; O'Brien, D. F.; Whitesides, T. H., Structural Effects on the Photo-Polymerization of Bilayer-Membranes. *J. Am. Chem. Soc.* **1982**, *104*, 305-307.
5. Davis, T. C.; Bang, J. J.; Brooks, J. T.; McMillan, D. G.; Claridge, S. A., Hierarchical Noncovalent Functionalization of 2D Materials by Controlled Langmuir-Schaefer Conversion. *Langmuir* **2018**, *34*, 1353-1362.
6. Bang, J. J.; Porter, A. G.; Davis, T. C.; Hayes, T. R.; Claridge, S. A., Spatially Controlled Noncovalent Functionalization of 2D Materials Based on Molecular Architecture *Langmuir* **2018**, *34*, 5454-5463.
7. Davis, T. C.; Bang, J. J.; Brooks, J. T.; McMillan, D. G.; Claridge, S. A., Correction To: Hierarchically Patterned Noncovalent Functionalization of 2D Materials by Controlled Langmuir–Schaefer Conversion. *Langmuir* **2018**, *34*, 2900.